Published in final edited form as:

Nat Microbiol. ; 2: 16199. doi:10.1038/nmicrobiol.2016.199.

An HIV-1 antibody from an elite neutralizer implicates the fusion peptide as a site of vulnerability

Marit J. van Gils[1,2,*,#], **Tom L.G.M. van den Kerkhof**[1,3,#], **Gabriel Ozorowski**[4], **Christopher A. Cottrell**[4], **Devin Sok**[2], **Matthias Pauthner**[2], **Jesper Pallesen**[4], **Natalia de Val**[4], **Anila Yasmeen**[5], **Steven W. de Taeye**[1], **Anna Schorcht**[1], **Stephanie Gumbs**[1], **Inez Johanna**[1], **Karen Saye-Francisco**[2], **Chi-Hui Liang**[2], **Elise Landais**[2], **Xiaoyan Nie**[6], **Laura K. Pritchard**[7], **Max Crispin**[7], **Garnett Kelsoe**[6], **Ian A. Wilson**[4], **Hanneke Schuitemaker**[3,8], **Per Johan Klasse**[5], **John P. Moore**[5], **Dennis R. Burton**[2,9], **Andrew B. Ward**[3], and **Rogier W. Sanders**[1,5,*]

[1]Department of Medical Microbiology, Academic Medical Center, University of Amsterdam, 1105 AZ Amsterdam, The Netherlands [2]Department of Immunology and Microbial Science, Scripps CHAVI-ID, IAVI Neutralizing Antibody Center and Collaboration for AIDS Vaccine Discovery (CAVD), The Scripps Research Institute, La Jolla, CA 92037, USA [3]Department of Experimental Immunology, Academic Medical Center, University of Amsterdam, 1105 AZ Amsterdam, The Netherlands [4]Department of Integrative Structural and Computational Biology, Scripps CHAVI-ID, IAVI Neutralizing Antibody Center and Collaboration for AIDS Vaccine Discovery (CAVD), The Scripps Research Institute, La Jolla, CA 92037, USA [5]Department of Microbiology and Immunology, Weill Medical College of Cornell University, New York, NY 10021, USA [6]Department of Immunology and Human Vaccine Institute, Duke University, Durham, NC 27710, USA [7]Oxford Glycobiology Institute, Department of Biochemistry, University of Oxford, Oxford, OX1 3QU, UK [8]Janssen Pharmaceutical Companies of Johnson & Johnson, Archimedesweg 4-6, 2301 CA Leiden, The Netherlands [9]Ragon Institute of Massachusetts General Hospital, Massachusetts Institute of Technology, and Harvard University, Cambridge MA 02139, USA

SUMMARY

The induction of broadly HIV-1 neutralizing antibodies (bNAbs), capable of neutralizing various viral strains, by vaccination is challenging, but understanding how a subset of HIV-infected individuals develops bNAbs may guide immunization strategies. Here, we describe the isolation and characterization of the bNAb ACS202 from an elite neutralizer that recognizes a new, trimer-specific and cleavage-dependent epitope at the gp120-gp41 interface of the envelope glycoprotein

[*]Corresponding authors. m.j.vangils@amc.uva.nl; r.w.sanders@amc.uva.nl.
[#]These authors contributed equally to this work

AUTHOR CONTRIBUTIONS

MJG, TLGMK, MC, GK, IAW, HS, PJK, JPM, ABW and RWS each contributed to the design of the study, analysis of the data, and preparation of this manuscript. MJG, DS and MP performed B-cell sorting. MJG, TLGMK, SWT, SG, IJ and KSF performed antibody cloning, neutralization assays, cell surface staining, and epitope mapping assays. MJG, TLGMK, SG and RWS designed and produced SOSIP trimers. GO, CAC, JP and NV performed the EM studies. CHL and XN performed the auto- and polyreactivity assays and LKP performed the glycan profile assays.

Competing financial interests

H. Schuitemaker is currently employed by Crucell Holland B.V., a Janssen pharmaceutical company of Johnson & Johnson and is a shareholder of Johnson & Johnson.

(Env), involving the glycan N88 and the gp41 fusion peptide. In addition, an Env trimer, AMC011 SOSIP.v4.2, based on early virus isolates from the same elite neutralizer, was constructed and its structure by cryo-EM at 6.2 Å resolution reveals a closed, pre-fusion conformation similar to that of the BG505 SOSIP.664 trimer. The availability of a native-like Env trimer and a bNAb from the same elite neutralizer provides the opportunity to design vaccination strategies aimed at generating similar bNAbs against a key functional site on HIV-1.

MAIN TEXT

An HIV-1 vaccine should ideally elicit broadly neutralizing antibodies (bNAbs) that can protect against acquisition of a wide variety of circulating viruses from different genetic subtypes [1]. The isolation of multiple bNAbs from HIV-1 infected individuals has revealed that the human immune system is capable of eliciting them [2–4] and their protective effect has been confirmed in macaque challenge studies (reviewed in [5]). Many HIV-1 infected individuals develop bNAbs to some level, and ~1% of infected people develop exceptionally broad and potent responses that are active against viruses from most genetic subtypes with high potency [3,6,7]. The latter group, termed “elite neutralizers”, exemplifies how the human B cell repertoire has the capability to respond effectively to the HIV-1 envelope glycoprotein (Env) trimer despite its extreme variation. Understanding how elite neutralizers raise these exceptionally broad and potent responses can guide the design of Env vaccines that present the same epitopes to the naïve immune system, particularly when we have information on the autologous Env trimers that induced the bNAbs.

bNAbs to viral pathogens were once thought to target a small and specific number of epitopes, but for HIV-1, they have now been shown to develop against most regions of the Env surface that retain some level of conservation, such as the trimer apex (sub-regions of V1V2 and V3), gp120 outer domain glycans (OD-glycans), gp120 CD4 binding site, gp120-gp41 interface, and the gp41 membrane proximal external region (MPER) (reviewed in [8]). By definition, these bNAb epitopes must be largely conserved and also accessible on many circulating primary viruses, in some cases from all the genetic subtypes. To date, however, no Env immunogen has been able to elicit bNAbs when tested in animals or humans. For an immunogen to elicit bNAbs it is necessary, but not sufficient, to present at least one bNAb epitope and preferably many of them. Soluble trimers, termed SOSIP proteins, are excellent antigenic mimics of virion-associated Env and express almost all of the known bNAb epitopes and, hence, are suitable frameworks for vaccine design [9,10]. bNAbs targeting the gp120-gp41 interface have only been recently identified [11–15]. They target distinct but overlapping epitopes with components on both gp120 and gp41. Furthermore, they often only bind to native-like trimers. As a consequence they are valuable tools for the validation of new trimeric Env vaccine candidates.

Several SOSIP trimers have now been described for multiple genetic subtypes [9,16–22]. Experiments in animals showed that, unlike earlier Env subunit protein designs, SOSIP trimers can elicit NAb responses against autologous, neutralization-resistant (Tier-2) viruses [22,23]. However, so far, they have not been able to raise broader responses against different strains and subtypes, indicating that improvements to the design or immunization

strategies are still needed. One possible strategy is to construct trimers based on *env* gene sequences that evolved in elite neutralizers over the course of natural infection to assess whether such immunogens can indeed induce the types of bNAbs that emerge during viral infection.

We sorted Env-specific memory B cells from PBMCs isolated at 40 months post-seroconversion (post-SC) from an elite neutralizer, D12950 (IDU2 in [24]), who was infected with a subtype B virus via injection drug use (IDU) and enrolled in the Amsterdam Cohort Studies on HIV-1 infection and AIDS (ACS) (Supplementary Figure 1). Single Env-specific memory B cells were sorted using three Avi-tagged and biotinylated Env protein probes: BG505 SOSIP.664-AviB trimer, 94UG103 gp120-AviB, and MGRM-C026 gp120-AviB. These probes were chosen because sera from D12950 very potently neutralized the parental BG505, 94UG103 and MGRM-C026 viruses (ID_{50} values of 484, 453 and 967, respectively, at 40 months post-SC) [24]. We sorted 240 HIV-specific memory B cells that recognized at least one of the Env probes. Among the memory B cells identified, ~3.7% recognized one or more of the Env probes; ~0.45% all three probes; ~1.34% only the trimer; ~ 1.35 % one or both of the gp120s but not the trimer; and ~0.56% the trimer and one of the gp120s (Figure 1A).

The 240 Env-specific memory B cells were individually sorted into lysis buffer, and their mRNA were reverse transcribed, amplified and sequenced to generate immunoglobulin G (IgG) heavy (IgH) and light (IgL) chain variable (V) genes [25]. We successfully amplified 70 heavy (H) chain, 38 light (L) chain kappa, and 84 light chain lambda BCR variable (V) region sequences resulting in 42 Ig H-L pairs. A maximum-likelihood tree constructed from the IgHV sequences showed that multiple clonal families were present (Supplementary Figure 2). Ab sequencing indicated a normal usage of heavy and light chain V genes (Figure 1B). Furthermore, The IgHV gene sequences were compared with antibody germline (GL) sequences (IMGT database [26]) and showed a normal distribution with an average identity of 90.8% to their putative GL (Figure 1C), and average CDRH3 length of 18 amino acids (Figure 1D).

From each of the different clonal families, we selected either one or multiple Ig H-L pairs and cloned them into expression vectors to produce mAbs. We successfully cloned 29 mAbs of which 17 showed both high-level IgG production and strong binding to BG505 SOSIP. 664 trimers in ELISA (Supplementary Table 1). Only one family of mAbs (ACS201–205) bound to the BG505 trimers but not to BG505 gp120 monomers, while all of the other mAbs recognized both Env proteins. Binding of BG505 mutant proteins in ELISA showed that mAbs ACS211–212 and ACS221 were V3-dependent, while ACS241–242 required D368 for binding, implying specificity for the CD4 binding site (CD4bs). The remaining 12 mAbs were neither V3 nor CD4bs dependent (Supplementary Table 1).

We then tested the neutralizing capacity of mAbs from each clonal family using an initial panel of 11 viruses from several subtypes. mAbs from multiple families neutralized Tier-1 viruses efficiently, but only the trimer-specific ACS201–205 family members could neutralize multiple Tier-2 viruses and they were more potent against Tier-2 than Tier-1 viruses (Supplementary Table 1). Among them, mAb ACS202 had the broadest and most

potent neutralization activity in this initial screen. We therefore tested it against a much larger panel of 75 viruses representing different genetic subtypes [27]. Here, ACS202 neutralized 34 of the viruses (45%), including ones from all represented subtypes, with a median IC_{50} value of 0.142 μg/ml (Figure 2 and Supplementary Table 2). ACS202 was particularly broad against clade C and recombinant CRF01_AE viruses, neutralizing 69% of these subtypes in the test panel, and 88% and 100% of chronic viruses within these subtypes, respectively. Similarly to many other bNAbs, particularly ones targeting the trimer apex or trimer stalk, ACS202 incompletely neutralized a subset of test viruses (Supplementary Figure 3A–B) [28,29]. When compared to five other bNAbs, ACS202's breadth was similar to PGT143 and VRC26.08, but less than PGV04, PGT121 and PGT151; its overall potency was in the middle of the range spanned by the bNAb test panel [30,31].

ACS202 is encoded by IgH V3-30*03, J6*02 and D2-8*02 genes, with V and J gene identities of 84% and 82% (nucleotide) to their respective GL genes, respectively, which are comparable to other HIV bNAbs (IgHV range 68–88% [32]). The IgL is encoded by IgLκ V1-33*01 and J3*01 genes with nucleotide identities of 79% and 97%, respectively. ACS202 has a long CDRH3 consisting of 24 amino acids that includes a motif of four successive tyrosine residues that is generally rare, but also present in PGT151, but not any other HIV bNAbs (Supplementary Figure 2B). Multiple tyrosine residues within the antigen-recognition site of Abs are often associated with polyreactivity and/or autoreactivity [33–35] and we found that ACS202 was indeed highly polyreactive (Supplementary Figure 4), in contrast to PGT151 [11,12].

We performed ELISA and SPR with various forms of BG505 Env protein to gain insights into the ACS202 epitope (Supplementary Figure 5A–D). In contrast to its strong interaction with the SOSIP.664 trimer, ACS202 reacted poorly or not at all with monomeric gp120, a gp41 construct, or a SOSIP.664 gp120-gp41 monomer (gp140). In addition, ACS202 showed poor binding to uncleaved non-native gp140 with or without a foldon trimerization domain, uncleaved "native flexible linker (NFL) gp140 [36], or uncleaved cell surface associated gp160 (Supplementary Figure 5E). The implication is that the ACS202 epitope is present only on cleaved, native-like trimers, a property shared with other gp120-gp41 interface bNAbs [11–15].

A panel of BG505 SOSIP.664 trimer mutants that lack specific glycan sites indicated that ACS202 binding was not sensitive to removal of glycans at positions 230, 234, 611, 625 or 637 (Supplementary Figure 5D). However, its binding was critically dependent on the glycan at position 88. A glycan site-specific analysis of the BG505 SOSIP.664 trimer shows that a complex glycan is usually present at position N88 [37]. When BG505 SOSIP.664 trimers were produced in cells that lack GlcNAc transferase I (GnT−/− cells), thereby preventing glycan processing, ACS202 binding was only slightly decreased (Supplementary Figure 5D). When virus was grown in the presence of kifunensine, an α-mannosidase I inhibitor that blocks glycan processing, neutralization by ACS202 was not affected (Supplementary Figure 5D). Hence, ACS202 binding is not influenced substantially by glycan processing, similar to what has been been observed for 35O22.

To further define the epitope, we next tested a set of 60 JR-CSF Env-pseudotyped virus mutants for their sensitivity to ACS202 (Figure 3 and Supplementary Table 3). The T90A

mutant virus that lacks the N88 glycan was completely resistant to ACS202 neutralization, which is consistent with the mutant trimer studies above. In contrast, deleting the topologically proximal glycans at positions 241 or 448 had no effect on ACS202 activity. Residues E83, V85, E87 and N229, all located close to the N88 glycan, were also found to be critical for ACS202 neutralization. Unexpectedly, ACS202 neutralization was also highly sensitive to substitutions of multiple residues in the fusion peptide (FP) and the fusion peptide proximal region (FPPR) of gp41 (Figure 3 and Supplementary Table 3).

SPR experiments involving bNAbs to defined epitopes showed that ACS202 competed strongly with PGT151, substantially with 35O22 and 3BC315, but not detectably with 8ANC195, VRC01 or PGT145 (Supplementary Figure 5F) [12,13,30,38,39]. As PGT151, 35O22, 3BC315 and 8ANC195 all target the gp120-gp41 interface, albeit at different locations, the SPR-competition data imply that ACS202 recognizes this general area of the trimer, perhaps nearest the PGT151 epitope, but most distant from 8ANC195. We noted that the BG505 sequence lacks the nearby glycan at position 241 which might influence accessibility to the area to which ACS202 binds. To test this, we performed additional SPR experiments with a BG505 SOSIP.664 S241N mutant. This mutant has a lower affinity for ACS202, indeed suggesting that the 241 glycan hinders access to the ACS202 epitope, explaining the high affinity of the original BG505 SOSIP.664 for ACS202 (Supplementary Figure 5C).

To gain additional insights into the ACS202 epitope, we produced soluble, recombinant SOSIP trimers (designated AMC011) based on the consensus sequence from early *env* genes (8 months post-SC) derived from the same D12950 elite neutralizer (Supplementary Figure 6A–B). The corresponding AMC011 virus showed a Tier-2 phenotype (Supplementary Table 4). The sequence modifications for the SOSIP.v4.2 trimer are summarized in the Methods and have been described elsewhere (see Supplementary Figure 6B) [9,16,17,22]. The AMC011 SOSIP.v4.2 Env proteins were produced by transient transfection of 293F cells followed by affinity chromatography with the trimer-specific PGT145 bNAb [22], yielding homogenous, cleaved trimers (Supplementary Figure 6C–D). When these PGT145-purified proteins were imaged using negative stain electron microscopy (NS-EM), the reference-free 2D class averages revealed trimers that consistently adopted a native-like conformation, with the three protomers closely associated with one another (Supplementary Figure 6E and Supplementary Table 5).

The differential scanning calorimetry (DSC) profile of the AMC011 SOSIP.v4.2 trimers, obtained with a two-state model, yielded a thermal denaturation (T_m) midpoint value of 63.0°C (Supplementary Figure 6F and Supplementary Table 5), which is consistent with those we have reported for SOSIP.664 and SOSIP.v4 trimers of various genotypes [9,17,20,22,40]. A hydrophilic interaction liquid chromatography-ultra performance liquid chromatography (HILIC-UPLC) analysis showed that the AMC011 SOSIP.v4.2 trimers predominantly expressed oligomannose glycans of the $Man_{5-9}GlcNAc_2$ type (75%), with $Man_8GlcNAc_2$ and $Man_9GlcNAc_2$ structures accounting for about half of the overall glycan population (Supplementary Figure 6G and Supplementary Table 5). The high oligomannose content is consistent with the glycan profile of BG505 SOSIP.664 trimers, and resembles virion-derived Env [41].

To further investigate the 3D-dimensional structure of AMC011 SOSIP.v4.2 trimers, we used cryo-EM to analyze their complex with bNAb PGV04 Fab. We obtained a 3D reconstruction at 6.2 Å resolution (Figure 4A and Supplementary Figure 7) and produced an atomic model using Rosetta. Density corresponding to many of the glycosylation sites was clearly visible in the reconstruction, including the N88 glycan involved in the ACS202 epitope and nearby glycans at positions N234, N241, and N448 (Figure 4B). Overlaying the AMC011 SOSIP.v4.2/PGV04 structure with that of BG505 SOSIP.664 (PDB: 5CEZ) showed that the two native-like soluble trimer variants were very similar to one another (Figure 4C). While V1V2 loop length differed between the two variants (longer V1 and shorter V2 in AMC011 versus BG505), those regions of the map were not resolved, likely due to flexibility.

An SPR-based antigenicity analysis showed that most bNAb epitopes were present on the AMC011 SOSIP.v4.2 trimers, including those for the trimer-specific bNAbs PGT145 and PGT151, whereas the V3- and CD4bs-associated epitopes for non-NAbs 19b and F105 were absent (Figure 5A). VRC01 binding is low for AMC011 SOSIP.v4.2, but the early virus isolates were also quite resistant to VRC01 (Supplementary Table 4). Overall, the AMC011 trimers are antigenically comparable to other native-like SOSIP trimers that we have described, in that they present multiple bNAb epitopes while occluding most non-NAb epitopes [9,16,17,20,22].

The AMC011 SOSIP.v4.2 protein and the ACS202 bNAb together provide a unique opportunity for studying how a trimer-specific bNAb interacts with the autologous, native-like trimer (i.e., one derived from the same donor). In SPR analyses, ACS202 bound slightly more strongly to the autologous AMC011 SOSIP.v4.2 trimer, compared to BG505 SOSIP.664, with $K_{D(app)}$ of 6.0 nM *vs.* 14.0 nM, respectively; the association kinetics were similar in both cases, but dissociation from the AMC011 trimers was slower (Figure 5B), which can explain the difference in neutralization IC_{50}. Similar effects of dissociation rates on neutralization potency have been noted for PGDM1400 family members [42]. The mAb:trimer stoichiometry was 3:1 (Supplementary Table 6). A low resolution NS-EM reconstruction confirms that the ACS202 Fab binds to the AMC011 SOSIP.v4.2 gp120-gp41 interface (Figure 5C and Supplementary Figure 8), and docking of published SOSIP models into the EM density indicates the epitope is proximal to the fusion peptide of gp41 (Figure 5D) with involvement of the N88 glycan [43]. SPR experiments with AMC011 SOSIP.v4.2 trimers corroborated the competition of ACS202 with PGT151, 35O22 and 3BC315 (Supplementary Figure 9A).

Next, we tested ACS202 binding to AMC011 SOSIP.v4.2 variants (Supplementary Figure 9B). The E87A and N88Q substitutions almost completely abrogated ACS202 binding to the autologous trimer, while the E83A and N229K substitutions had a partial effect, confirming the importance of the area around glycan N88 (Supplementary Figure 9B). Furthermore, substitutions A512W, I515W, G516W and S528W reduced ACS202 binding substantially, further supporting the role of the fusion peptide. Thus, these mutagenesis data, using the autologous AMC011 trimer, confirmed our observations obtained with the JR-CSF virus and BG505 trimer.

To ascertain whether the month 8 consensus AMC011 sequence was a reasonable approximation of the virus that triggered the ACS202 lineage, we generated infectious molecular clones of the individual viruses on which the AMC011 consensus sequence was based and performed neutralization experiments (Supplementary Table 4). The results show that one clone (clone 2G9) was sensitive to ACS202, as was the consensus virus. In contrast, the other two clones were resistant to ACS202 (clones 2D6 and 2D7). One explanation is that (a predecessor of) the sensitive clone triggered the induction of the ACS202 lineage, which in turn caused viral escape, as exemplified by the two resistant clones. Interestingly, the converse result was obtained with 35O22. Thus, the 2D6 and 2D7 clones that were resistant to ACS202 were sensitivity to 35O22, while the 2G9 clone and the consensus virus were resistant to 35O22. The different neutralization sensitivities of the AMC011 viruses in combination with their sequence alignment allowed us to look for AMC011 sequence determinants for sensitivity and resistance to both ACS202 and 35O22. Residue 87 stands out in the alignment (Supplementary Figure 6A). Thus, the two AMC011 viruses (and also BG505) that were sensitive to ACS202 but relatively resistant to 35O22 have a glutamic acid at position 87 (E87). In contrast, the two AMC011 viruses that were resistant to ACS202 and more sensitive to 35O22 have a lysine or a glycine at position 87 (K87, G87). These results are concordant with the mutagenesis data describe above in which the E87A substitution abrogated ACS202 binding to AMC011 SOSIP.v4.2 as well as ACS202 neutralization of the JR-CSF virus (Figure 3 and Supplementary Figure 9B), and suggest that the AMC011 SOSIP.v4.2 is representative of the autologous Env that induced the ACS202 lineage. In contrast, the clones containing the E87K or E87G substitutions, might represent escape viruses.

The ACS202 epitope is distinct from other known gp120-gp41 interface bNAbs. While 35O22 also binds the N88 glycan, its epitope involves other glycans at N241, N230 and N625. In addition, the ACS202 epitope is dependent on Env cleavage, a property shared with PGT151 but not 35O22. 3BC315 also binds proximal to glycan N88, but its Fab is rotated by 90° (i.e. planar to the membrane) relative to ACS202. Furthermore, in comparison to 3BC315 and PGT151, docking the EM density of ACS202 (from the complex with AMC011.v4.2 SOSIP) onto a high-resolution x-ray structure of BG505 SOSIP.664 [18,19] suggests a greater interaction with gp120 residues and glycans, particularly N88, and contact with the gp41 fusion peptide and the fusion peptide proximal region (Figure 3E). In contrast, 3BC315 and PGT151 interact more with gp41 than ACS202, while PGT151 also depends on the N611 and N637 glycans. Overall, the ACS202 epitope partially overlaps with the other gp120-gp41 interface bNAbs PGT151, 35O22 and 3BC315 epitopes, but not with 8ANC195, consistent with the SPR competition assay (Supplementary Figure 9A), but has a markedly different epitope footprint (Figure 5E).

Thus, ACS202 shares some similarities with PGT151 such as interaction at the gp120-gp41 interface and presence of a hydrophobic YYYY motif in its CDRH3, which is predicted to interact with the fusion peptide [44]. We can speculate that the YYYY motif in ACS202 also mediates the interaction with the fusion peptide. In contrast, bNAbs 3BC315 and VRC34, which are also predicted to bind the fusion peptide, do not have an YYYY motif, suggesting that there are different solutions for the interaction with the fusion peptide [11,14,15]. PGT151 binds Env at a stoichiometry of 2 Fabs per trimer due to allosteric changes induced upon

antibody binding, preventing binding of a third Fab to bind [37]. For ACS202, the stoichiometry of 3 Fabs per trimer further emphasizes that ACS202 and PGT151 do not engage Env in a similar manner.

When the neutralization breadth of ACS202 and the serum from the elite neutralizer [24] are compared, it is clear that ACS202 alone does not fully recapitulate the overall properties of the serum, which neutralized additional viruses [24]. Hence, either more active members of the ACS202 family remain to be identified, or other as yet unknown bNAb specificities are also present. Nevertheless, the isolation and characterization of a novel bNAb ACS202 from an elite neutralizer reveals the fusion peptide is a site of vulnerability that, when combined with construction of a soluble recombinant, native-like SOSIP trimer derived from the same elite neutralizer, serves as a scaffold to attempt to induce similar bNAbs by vaccination.

MATERIALS AND METHODS

Human specimens

Peripheral blood mononuclear cells (PBMCs) were obtained from donor D12950 [24], an HIV-1 infected male participant in the Amsterdam Cohort Studies on HIV-1 infection and AIDS (ACS). The ACS accords to the ethical principles set out in the Declaration of Helsinki. Written consent was obtained prior to data collection. The present study was approved by the Academic Medical Center's Institutional Medical Ethics Committee. Individual D12950 was infected with an HIV-1 subtype B virus via injection drug use (IDU). When the individual joined the ACS, the subject was HIV-1 negative but seroconverted while being monitored as a cohort member and has now been under clinical observation for >20 years. The $CD4^+$ T-cell numbers had declined (average 390 cells/μl; range 230–570) but detectable viral loads (average log4.4) were detected until commencement of antiretroviral therapy ~9 years post-SC, but no clinical signs of AIDS in D12950 (Supplementary Figure 1A). In addition, D12950 had no protective HLA-type and was homozygous for the WT CCR5 gene (i.e. no Δ32 deletion was present). D12950 has been previously described in a report of the longitudinal development of bNAbs in elite neutralizers, and was recorded there as individual IDU2 [24]. Serum and peripheral blood mononuclear cell (PBMC) samples were taken from D12950 every ~4 months. The *env* gene sequences used to make the AMC011 SOSIP.v4.2 trimers were derived from clonal isolates obtained at 8 months post-SC, using serial diluted PBMCs co-cultivated with PHA-stimulated PBMC of healthy donors, as described previously [46], while the mAbs, including ACS202, were derived from a blood sample taken at 40 months post-SC (Supplementary Figure 1B).

Design of AMC011 SOSIP.v4.2 trimers

The *env* genes from the three clonal variants were used to obtain a consensus sequence, with a cut-off of ≥60% for an amino acid at a specific position. The consensus sequence was used to generate the AMC011 SOSIP.v4.2 construct, following published methods [9,22]. In brief, we introduced the A501C and T605C (HXB2 numbering system) substitutions to make the disulfide bond linking gp120 to gp41; the I559P, L543Q and Q567K trimer-stabilizing changes in gp41; the hexa-arginine furin cleavage site at the C-terminus of gp120 to enhance cleavage; a tissue plasminogen activator (tPA) signal peptide replacing the natural Env signal

peptide to improve secretion; and a stop codon at position 664 to prevent aggregation [9,16,17,22]. The design was then further refined by the introduction of changes H66R and A316W, resulting in the SOSIP.v4.2 construct. For some uses, a His-tag was introduced at the C-terminus of $gp41_{ECTO}$ [9].

Env protein production

For this study, we also used untagged, Avi-tagged, or His-tagged BG505 SOSIP.664 trimers. In addition, we used Avi-tagged monomeric gp120 from isolates 94UG103, MGRM-C026 and BG505 (all containing an L111A substitution to reduce dimerization [47]), as well as various mutant BG505 gp120 proteins, as described previously [23]. Recombinant Env proteins were expressed in HEK293F cells (Invitrogen) as described previously [9,18]. HEK293F cells were not authenticated in the laboratory but were periodically tested for mycoplasma contamination. Briefly, HEK293F cells were maintained in FreeStyle medium (Invitrogen), seeded at a density of 1×10^6/ml and transfected using 1 mg (1mg/ml) of 293Fectin (Invitrogen) or PEImax (1.0 mg/ml; 936 μg) with 300 μg of Env plasmid and (for making SOSIP trimers) 75 μg of furin plasmid in OPTI-MEM, according to the manufacturer's protocol. In some cases, glycan-modified proteins were produced by adding 25 μM kifunensine to the cells on the day of transfection. Culture supernatants were harvested 6–7 days after transfection. SOSIP trimers were purified by affinity chromatography using a 2G12 or PGT145 column as described previously [17,22]. Monomeric gp120 proteins were purified using a *Galanthus nivalis* lectin (Vector Labs) column [9]. The eluted Env proteins were concentrated using Vivaspin columns with a 100-kDa cut off (GE Healthcare). The 2G12 affinity-purified Env proteins were further purified to size homogeneity using size exclusion chromatography (SEC) on a Superose 6 10/300 GL column (GE Healthcare) in PBS. The desired fractions were collected and pooled, and protein concentrations were determined using UV_{280} absorbance using theoretical extinction coefficients derived with Expasy (Protparam Tool). The Avi-tagged proteins were biotinylated using the BirA enzyme (Aviditiy) according to the manufacturer's protocol. The resulting biotinylated proteins are referred to using the descriptor AviB.

Single B cell sorting by flow cytometry

Sorting was performed as described previously [42]. In brief, donor PBMCs were stained with primary fluorophore-conjugated antibodies to human CD3, CD8, CD14, CD19, CD20, CD27, IgG and IgM (BD Pharmigen). For staining with Env proteins, 50 nM of BG505 SOSIP.664-AviB, 94UG103 gp120-AviB or MGRM-C026 gp120-AviB were coupled in equimolar ratios to Streptavidin-APC (Life Technologies), Streptavidin-BV785 (Biolegend) or Streptavidin-PE (Life Technologies), respectively. Cells were stained for 1 h at 4°C in PBS supplemented with 1 mM EDTA and 1% FBS. In the gating strategy, we first excluded unwanted cell populations ($CD3^-/CD8^-/CD14^-$) followed by selection of HIV Env-specific (positive for any of the 3 probes) memory B cells ($CD19^+/CD20^+/IgG^+/IgM^-/HIV^+$). Cells of interest were single-cell sorted using a BD FACSAria III machine, into 96-well plates containing lysis buffer, and immediately stored at −80°C.

Single B cell RT-PCR, gene amplification, and cloning

Reverse transcription and subsequent PCR amplification of IgG heavy and light chain variable genes (VH and VL, respectively) were performed according to previous protocols [25,38]. All PCR reactions were performed in a 25 μl volume with 2.5 μl of cDNA transcript using HotStar Taq DNA polymerase master mix (Qiagen). Primer sets used for gene amplification have been described elsewhere [25]. Amplified IgG VH and VL regions were sequenced and analysed using the IMGT V-quest webserver (www.IMGT.org) [26]. Wells for which VH and VL (kappa and lambda) sequences were deemed productive re-arrangements by IMGT analysis were selected for cloning into corresponding Igγ1, Igκ and Igλ expression vectors as previously described [38]. The Ab naming system takes into account the ACS patient identifier (D12950, also known as ACS2), the clonal family (0–9) and the number of the individual clone, an example being ACS2 family-0 clone-1 = ACS201.

Antibody production

293F cells (Invitrogen) were co-transfected with heavy and light chain plasmids (1:1 ratio) using PEImax. Transfections were performed according to the manufacturer's protocol and Ab supernatants were harvested four days following transfection. Abs were further purified using a protein A/G column (ThermoFisher Scientific) as described previously [42].

D7324-capture ELISA for gp140 SOSIP.664-D7324 proteins

ELISAs were performed as described previous [9,10]. Briefly, Microlon 96-wells plates (Greiner Bio-One, Alphen aan den Rijn, The Netherlands) were coated overnight with mAb D7324 (Alto Bioreagents, Dublin, Ireland) at 10 μg/ml in 0.1 M $NaHCO_3$, pH 8.6 (50 μl/well). After washing and blocking steps, purified D7324-tagged SOSIP proteins (5 μg/ml) were added in TBS/10% FCS for 2 h. Unbound proteins were washed away by 2 wash steps, and TBS (150 mM NaCl, 20 mM Tris) plus 2% skimmed milk was added to further block non-specific protein-binding sites. Serially diluted mAbs or CD4-IgG2 in TBS/2% skimmed milk were then added for 2 h followed by 3 washes with TBS. In some cases, sCD4 (1 μg/ml) was added during the incubation with a mAb. Horseradish peroxidase labeled goat-anti-human immunoglobulin G (IgG) (Jackson Immunoresearch, Suffolk, England) was added for 1 h at a 1:3000 concentration in TBS/2% skimmed milk, followed by 5 washes with TBS/0.05% Tween-20. Colorimetric detection was performed using a solution containing 1% 3,3′,5,5′-tetramethylbenzidine (Sigma-Aldrich, Zwijndrecht, The Netherlands), 0,01% H_2O_2, 100 mM sodium acetate and 100 mM citric acid. Color development was stopped using 0.8 M H_2SO_4 after 5 min, and absorption was measured at 450 nm.

TZM-bl based neutralization assays

Neutralization experiments were carried out as described previously [10]. In summary, one day prior to infection, TZM-bl cells (NIH AIDS reagent program) were plated on a 96-well plate in DMEM containing 10% FCS, 1× MEM nonessential amino acids, penicillin and streptomycin (both at 100 U/ml), and incubated at 37°C in an atmosphere containing 5% CO_2. TZM-bl cells were not authenticated in the laboratory but were periodically tested for mycoplasma contamination. Virus (500 pg) was incubated for 30 min at room temperature

with threefold serial dilutions of monoclonal antibodies. This mixture was added to the cells and 40 μg/ml DEAE, in a total volume of 200 μl. Two days later, the medium was removed and lysed in Reporter Lysis Buffer (Promega, Madison, WI). Luciferase activity was measured using a Luciferase Assay kit (Promega, Madison, WI) and a Glomax Luminometer according to the manufacturer's instructions (Turner BioSystems, Sunnyvale, CA). Uninfected cells were used to correct for background luciferase activity. Nonlinear regression curves were determined and IC_{50} values were calculated using a sigmoid function in Graphpad Prism v5.01.

Cell surface associated Env binding

Cell surface gp160 binding was tested using flow cytometry as previously described [12]. Briefly, 3-fold serial dilutions of monoclonal antibodies starting at 50 μg/ml were added to HEK293T cells (ATCC) that were transfected 2 days prior with a plasmid encoding JR-FL wild-type gp160 or a gp160 that cannot be cleaved (REKR replaced with SEKS) and incubated for 1 h at RT. HEK293T cells were not authenticated in the laboratory but were periodically tested for mycoplasma contamination. The plate was washed twice with PBS and stained with a 1:50 dilution of R-phycoerythrin-Cy7 (PE-Cy7)-conjugated mouse anti-human IgG (BD Pharmigen). Binding was analyzed with flow cytometry as previously described [12].

Electron microscopy and image processing

For negative-stain analysis, AMC011 SOSIP.v4.2 trimers were expressed in HEK293F cells (Invitrogen) and purified by PGT145-affinity chromatography as described above and incubated with a 10-molar excess of ACS202 Fab previously produced using papain digestion of recombinant IgG. Incubations were carried out overnight at room temperature and the complex was diluted to ~0.03 mg/mL prior to application onto a carbon-coated 400 Cu mesh grid that had been glow discharged at 20 mA for 30 s. The grids were stained with 2% (w/v) uranyl formate for 60 seconds. Samples were imaged on an FEI Talos electron microscope operating at 200 keV, with an electron dose of ~ 25 e-/$Å^2$ and a magnification of 73,000× that resulted in a pixel size of 1.98 Å at the specimen plane. Automated data collection and initial data processing is similar to those methods described in [22]. 3D classification was performed using Relion [48] with an EM volume created from the x-ray structure of ligand-free BG505 SOSIP.664 (PDB: 4zmj) low pass filtered to 60 Å as the reference model. 3D classification suggested mostly full stoichiometry of binding (3 Fabs per trimer), and the most complete 3D model was then used as the initial model (low pass filtered to 40 Å) for further refinement using Relion, with C3 symmetry imposed and a total of 11,913 particles. The final resolution of the map using a Fourier shell correlation of 0.5 is estimated as ~21 Å.

For the cryo-EM data, A 5 μL aliquot of the purified complex (4.45 mg/mL) was incubated with 1 μL of 1.8mM DDM solution. At 4°C, 3 μL of this mixture was applied to the carbon face of a CF-2/2-4C C-Flat grid (Electron Microscopy Sciences, Protochips, Inc.), which had been plasma cleaned for 5 seconds using a mixture of Ar/O_2 (Gatan Solarus 950 Plasma system). The grid was then manually blotted and immediately plunged into liquid ethane using a manual freeze plunger. Micrographs were collected using previously described

methods [14] on an FEI Titan Krios operating at 300 kV mounted with a Gatan K2 direct electron detector. Each micrograph was collected in counting mode at 22,500× nominal magnification resulting in a calibrated pixel size of 1.31 Å/pix at the object level. A dose rate of ~10 e^-/((cam pix)*s) was used; exposure time was 200 ms per frame. The data collection resulted in a total of 3480 micrographs. Total dose for these micrographs was 40 $e^-/Å^2$. The nominal defocus range used was −1.0 to −4.5 μm.

Methods for frame alignment, CTF corrections, automated particle picking, stack creation, and initial reference-free 2D classification are described elsewhere [14]. After 2D classification, unbinned selected particles were refined against a density map at 60 Å resolution of ligand-free BG505 Env trimer purified from 293S cells (PDB: 4zmj). 3D classification was then performed in RELION version 1.4b1 resulting in six classes [48,49]. Density maps corresponding to 4 of the 6 classes (Supplementary Figure 7) proved to be of identical stoichiometries characterized by having three copies of PGV04 Fab complexed to the AMC011 SOSIP.v4.2 trimer. The particles from the 4 classes were merged for further refinement under C3 symmetry constraint followed by particle polishing and refinement of the resulting realigned, B-factor-weighed and signal-integrated particles. The resolution of the final map was 6.2Å at an FSC cut off of 0.143. The FSC was calculated using a soft-edged mask with a Gaussian falloff, encompassing the entire structure, including the Fab constant regions.

An initial model of AMC011 SOSIP.v4.2 was generated using the Modeller homology modelling tool in UCSF Chimera and the BG505 SOSIP.664 structure (PDB: 5CEZ) as a template [45,50,51]. The AMC011 SOSIP.v4.2 initial model was docked into the AMC011 SOSIP.v4.2/PGV04 map along with the Fv region of PGV04 (PDB: 3J5M) [17]. The resulting model was refined with Rosetta density-guided iterative local refinement using the AMC011 SOSIP.v4.2/PGV04 map as a spatial constraint while imposing C3 symmetry [52]. Rosetta output models were clustered based on pairwise RMSD using a cluster radius of 2.0 Å. The final structure was determined by selecting the model with the lowest MolProbity score from the largest cluster [53].

Differential scanning calorimetry (DSC)

Thermal denaturation was probed with a Nano DSC calorimeter (TA Instruments) as described previously [22]. Protein concentration was adjusted to 0.16 mg/ml. After loading the protein sample (110 μg) into the cell, thermal denaturation was probed at a scan rate of 1°C/min. Buffer correction, normalization and baseline subtraction procedures were applied before the data were analysed using NanoAnalyze 3.1.2 software. We report the midpoint of thermal denaturation (T_m) value of the SOSIP proteins derived from a two-state model (Supplementary Table 5).

Glycan profiling

Glycan profiling was performed as described previously [22]. Briefly, released glycans from Env proteins (5.5 μg) were resolved by hydrophilic interaction liquid chromatography-ultra performance liquid chromatography (HILIC-UPLC) using a 2.1 mm × 10 mm Acquity BEH Amide Column (1.7 μm particle size) (Waters, Elstree, UK). Fluorescence was measured

using an excitation wavelength of 250 nm and a detection wavelength of 428 nm. Data processing was performed using Empower 3 software. The percentage abundance of oligomannose-type glycans was calculated by integration of the relevant peak areas before and after Endoglycosidase H digestion, following normalization. Digestions were performed on free glycans at 37°C for 16 h.

Surface Plasmon Resonance (SPR)

Ab binding to immobilized Env proteins was performed as previously described [10,54] with some modifications. All experiments were performed at 25°C. In all experiments, HBS-EP (10 mM HEPES [pH 7.4], 150 mM NaCl, 3 mM EDTA, 0.002% P20 surfactant) was used as running buffer (GE Healthcare) at maximum flow rate (50 μl/min). At the end of each cycle, the sensor surface was regenerated by a single pulse with 10 mM glycine (pH 2.0) for 120 s. For the binding of a panel of Abs to AMC011 SOSIP.v4.2 protein, His-tagged proteins were captured at RL ~500–530 RU on anti-His CM5 sensor chips. IgGs of VRC01, 3BNC60, F105, PGT121, 19b, PG16, PGT145, PGT151, ACS202, 35O22, and 3BC315 were injected individually at 500 nM for 300 s and allowed to dissociate for 600 s. For a comparison of ACS202 IgG binding to the BG505 SOSIP.664 trimer, gp120-gp41$_{ECTO}$ protomer and gp120 monomer, D7324-epitope tagged proteins were immobilized on D7324-CM5 sensor surfaces to RL ~500–530 RU as previously described [48]. Binding of ACS202 IgG (500 nM) was monitored for 300 s of association and 600 s of dissociation. For kinetic modelling, ACS202 Fab was injected at 1 μM as the highest concentration and titrated down to 15.6 nM in two-fold dilution steps for kinetic analysis. In each cycle, association was monitored for 300 s and dissociation for 600 s. For each cycle fresh Env was immobilized on an anti-His Ab surface to 500 ± 10 RU. The Langmuir and conformational-change models were compared and the fits were uniformly superior with the latter, which was corroborated by an injection-time test. The reported parameters were obtained by global fits of the conformational-change model, in which $K_{d(app)}=((k_{on}/k_{off})*(1+(k_f/k_b)))^{-1}$. The values of the forward- and backward-conversion rate constants, k_f and k_b, respectively, were not reported; only those of the apparent dissociation constant, $K_{d(app)}$, the on-rate constant, k_{on} , the off-rate constant, and S_m, the stoichiometric number, were reported. One significant digit is given for the stoichiometric estimates, because of uncertainties stemming from the slanting plateau of the conformational change model and imprecision of the mass of the trimers related to heterologous glycosylation.

Competition between Abs for binding to Env proteins was measured as previously described [10]. The His-tagged BG505 SOSIP.664 protein was immobilized to anti-His CM5 sensor chips at ~500–520 RU. Abs were sequentially injected for binding to protein in the same cycle. The concentrations of the Abs were approximated so as to give near complete self-competition (ACS202 at 1 μM, VRC01 at 1 μM, 8ANC195 at 1.5 μM, PGT151 at 500 nM, 35O22 at 1 μM, and 3BC315 at 1 μM). The first Ab (Competitor) was injected for 200 s immediately followed by the second Ab (Analyte), both at a flow rate of 30 μl/min. Dissociation was followed for 300s at the end of the second injection. The residual binding was calculated as [(Response difference at 200 s for a second Ab)/(Response difference at 200 s for the same Ab as a single Ab)]* 100 (%).

Antibody polyreactivity assay

Abs were screened for reactivity with a diverse set of antigens on protein microarrays following the manufacturer's instructions and as described previously [34,55]. Briefly, ProtoArray microarrays (Invitrogen) were blocked and incubated on ice with 2 μg/ml of MAbs ACS201 and ACS202 or isotype control Ab 151K for 90 min. Ab binding to array proteins was detected with 1 μg/ml of Alexa Fluor 647-labeled anti-human IgG (Invitrogen) secondary Ab. The ProtoArray microarrays were scanned using a GenePix 4000B scanner (Molecular Devices) at a wavelength of 635 nm, with 10 μm resolution, using 100% power and 650 gain. Fluorescence intensities were quantified with GenePix Pro 5.0 program (Molecular Devices) using lot-specific protein location information provided by the microarray manufacturer.

The Anti-Nuclear Antibodies by Immunofluorescent Assay (ANA IFA) was performed using kits purchased from Aesku Diagnostics (Oakland, CA). These Aesku slides use optimally fixed human epithelial (HEp-2) cells as substrate and affinity purified, FITC-conjugated goat anti-human IgG for the detection. Procedure was followed according to the manufacturer's instructions. Slides were viewed at 20× magnification and photographed on an EVOS f1 fluorescence microscope at a 250 ms exposure with 100% intensity.

Single antigen enzyme immunoassays (EIAs) for SSA/Ro, SS-B/La, Sm, ribonucleoprotein (RNP), Jo-1, double-stranded DNA, centromere B, and histones were purchased from Aesku Diagnostics (Oakland, CA). The 96 wells are separately coated with these eight cellular and nuclear antigens for the qualitative detection of mAbs reactivity. The cut-off calibrator was provided by the manufacturer.

Anti-Cardiolipin Screen ELISA kit (Diamedix Corp, Miami Lakes, FL) was applied to test for mAb cardiolipin reactivity according the manufacturer's instructions. Antibodies were used at dilutions starting at 50 μg/ml and titrated in two fold serial dilutions. Positive control, negative controls, and standards for cut-off establishment, were provided by the manufacturer.

Monoclonal antibodies were screened for reactivity with soluble membrane proteins (SMP) and solubilized cytosolic proteins (SCP) as described previously [56] with a small modification. Briefly, SMP and SCP were extracted from CHO cells. The protein concentration was determined using the Dc-protein assay kit (BioRad). SMP and SCP were then immobilized on ELISA plate for mAbs screening. The results were established by reading the absorbance at 450 nm of the examined samples.

Data availability

The data that support the findings of this study are available from the corresponding author upon request. EM reconstructions have been deposited in the Electron Microscopy Data Bank under the accession numbers EMD-8299 and EMD-8302. IgHV and IgLV sequences of ACS201–205 have been deposited in Genbank under the accession numbers KX60465-KX60474.

Supplementary Material

Refer to Web version on PubMed Central for supplementary material.

Acknowledgments

The Amsterdam Cohort Studies (ACS) on HIV infection and AIDS, a collaboration between the Amsterdam Health Service, the Academic Medical Center of the University of Amsterdam, Sanquin Blood Supply Foundation, and the Jan van Goyen Clinic, are part of The Netherlands HIV Monitoring Foundation and are financially supported by the Center for Infectious Disease Control of The Netherlands National Institute for Public Health and the Environment. M.J.G is a recipient of a Dutch Aids Fonds (grant #2012041) and EMBO short-term fellowship (ASTF 260–2013). R.W.S. is a recipient of a Vidi grant from the Netherlands Organization for Scientific Research (grant #917.11.314) and a Starting Investigator Grant from the European Research Council (ERC-StG-2011-280829-SHEV). This work was also supported by the Vici grant to H.S. from The Netherlands Organization for Scientific Research (grant #918.66.628), the International AIDS Vaccine Initiative through the Neutralizing Antibody Consortium SFP1849 (D.R.B., A.B.W.), NIH R01 AI033292 (D.R.B.), NIH P01 AI110657 (J.P.M., A.B.W., I.A.W. R.W.S.), NIH R37 AI36082 (J.P.M.), Center for HIV/AIDS Vaccine Immunology and Immunogen Discovery Grant UM1AI100663 (D.R.B., A.B.W., I.A.W.), Collaboration for AIDS Vaccine Development (CAVD) grants OPP1111923 and OPP1132237 (J.P.M. and R.W.S.) and OPP1115782 (A.B.W.) from the Bill and Melinda Gates Foundation, and European Union's Horizon 2020 research and innovation programme under grant agreement No. 681137 (R.W.S). Funding was also provided by the NIH Interdisciplinary Training Program in Immunology 5T32AI007606-10 (D.S.).

We thank Dennis Burton, Michel Nussenzweig, and John Mascolla for providing bNAbs.

References

1. Burton DR, Mascola JR. Antibody responses to envelope glycoproteins in HIV-1 infection. Nature immunology. 2015; 16:571–576. DOI: 10.1038/ni.3158 [PubMed: 25988889]
2. Doria-Rose NA, et al. Frequency and phenotype of human immunodeficiency virus envelope-specific B cells from patients with broadly cross-neutralizing antibodies. J Virol. 2009; 83:188–199. [PubMed: 18922865]
3. Simek MD, et al. HIV-1 Elite Neutralizers: Individuals with Broad and Potent Neutralizing Activity Identified Using a High Throughput Neutralization Assay Together with an Analytical Selection Algorithm. J Virol. 2009; 83:7337–7348. [PubMed: 19439467]
4. Euler Z, Schuitemaker H. Cross-reactive broadly neutralizing antibodies: timing is everything. Frontiers in immunology. 2012; 3:215. [PubMed: 22833745]
5. van Gils MJ, Sanders RW. In vivo protection by broadly neutralizing HIV antibodies. Trends Microbiol. 2014; 22:550–551. S0966-842X(14)00174-7 [pii]; DOI: 10.1016/j.tim.2014.08.006 [PubMed: 25169020]
6. Sather DN, et al. Factors associated with the development of cross-reactive neutralizing antibodies during human immunodeficiency virus type 1 infection. J Virol. 2009; 83:757–769. [PubMed: 18987148]
7. Moore PL, Williamson C, Morris L. Virological features associated with the development of broadly neutralizing antibodies to HIV-1. Trends in microbiology. 2015; 23:204–211. DOI: 10.1016/j.tim.2014.12.007 [PubMed: 25572881]
8. Wibmer CK, Moore PL, Morris L. HIV broadly neutralizing antibody targets. Current opinion in HIV and AIDS. 2015; 10:135–143. DOI: 10.1097/COH.0000000000000153 [PubMed: 25760932]
9. Sanders RW, et al. A next-generation cleaved, soluble HIV-1 Env Trimer, BG505 SOSIP.664 gp140, expresses multiple epitopes for broadly neutralizing but not non-neutralizing antibodies. PLoS Pathog. 2013; 9:e1003618. PPATHOGENS-D-13-01512 [pii]. [PubMed: 24068931]
10. Derking R, et al. Comprehensive antigenic map of a cleaved soluble HIV-1 envelope trimer. PLoS pathogens. 2015; 11:e1004767. [PubMed: 25807248]
11. Blattner C, et al. Structural delineation of a quaternary, cleavage-dependent epitope at the gp41-gp120 interface on intact HIV-1 Env trimers. Immunity. 2014; 40:669–680. DOI: 10.1016/j.immuni.2014.04.008 [PubMed: 24768348]

12. Falkowska E, et al. Broadly neutralizing HIV antibodies define a glycan-dependent epitope on the prefusion conformation of gp41 on cleaved envelope trimers. Immunity. 2014; 40:657–668. S1074-7613(14)00123-X [pii]. DOI: 10.1016/j.immuni.2014.04.009 [PubMed: 24768347]
13. Huang J, et al. Broad and potent HIV-1 neutralization by a human antibody that binds the gp41-gp120 interface. Nature. 2014; 515:138–142. DOI: 10.1038/nature13601 [PubMed: 25186731]
14. Lee JH, de Val N, Lyumkis D, Ward AB. Model Building and Refinement of a Natively Glycosylated HIV-1 Env Protein by High-Resolution Cryoelectron Microscopy. Structure. 2015; 23:1943–1951. DOI: 10.1016/j.str.2015.07.020 [PubMed: 26388028]
15. Kong R, et al. Fusion peptide of HIV-1 as a site of vulnerability to neutralizing antibody. Science. 2016; 352:828–833. DOI: 10.1126/science.aae0474 [PubMed: 27174988]
16. Julien JP, et al. Design and structure of two HIV-1 clade C SOSIP.664 trimers that increase the arsenal of native-like Env immunogens. Proceedings of the National Academy of Sciences of the United States of America. 2015; 112:11947–11952. DOI: 10.1073/pnas.1507793112 [PubMed: 26372963]
17. Pugach P, et al. A native-like SOSIP.664 trimer based on an HIV-1 subtype B env gene. Journal of virology. 2015; 89:3380–3395. DOI: 10.1128/JVI.03473-14 [PubMed: 25589637]
18. Julien JP, et al. Crystal Structure of a Soluble Cleaved HIV-1 Envelope Trimer. Science. 2013 science.1245625 [pii].
19. Lyumkis D, et al. Cryo-EM Structure of a Fully Glycosylated Soluble Cleaved HIV-1 Envelope Trimer. Science. 2013 science.1245627 [pii].
20. Guenaga J, et al. Well-ordered trimeric HIV-1 subtype B and C soluble spike mimetics generated by negative selection display native-like properties. PLoS pathogens. 2015; 11:e1004570. [PubMed: 25569572]
21. Andrabi R, et al. Identification of Common Features in Prototype Broadly Neutralizing Antibodies to HIV Envelope V2 Apex to Facilitate Vaccine Design. Immunity. 2015; 43:959–973. DOI: 10.1016/j.immuni.2015.10.014 [PubMed: 26588781]
22. de Taeye SW, et al. Immunogenicity of Stabilized HIV-1 Envelope Trimers with Reduced Exposure of Non-neutralizing Epitopes. Cell. 2015; 163:1702–1715. DOI: 10.1016/j.cell.2015.11.056 [PubMed: 26687358]
23. Sanders RW, et al. HIV-1 VACCINES. HIV-1 neutralizing antibodies induced by native-like envelope trimers. Science. 2015; 349:aac4223. science.aac4223 [pii]. [PubMed: 26089353]
24. van den Kerkhof TL, et al. Early development of broadly reactive HIV-1 neutralizing activity in elite neutralizers. AIDS. 2014; 28:1237–1240. DOI: 10.1097/QAD.0000000000000228 [PubMed: 24556870]
25. Tiller T, et al. Efficient generation of monoclonal antibodies from single human B cells by single cell RT-PCR and expression vector cloning. Journal of immunological methods. 2008; 329:112–124. DOI: 10.1016/j.jim.2007.09.017 [PubMed: 17996249]
26. Lefranc MP, et al. IMGT, the international ImMunoGeneTics information system. Nucleic acids research. 2009; 37:D1006–1012. DOI: 10.1093/nar/gkn838 [PubMed: 18978023]
27. Seaman MS, et al. Tiered categorization of a diverse panel of HIV-1 Env pseudoviruses for assessment of neutralizing antibodies. J Virol. 2010; 84:1439–1452. [PubMed: 19939925]
28. McCoy LE, et al. Incomplete Neutralization and Deviation from Sigmoidal Neutralization Curves for HIV Broadly Neutralizing Monoclonal Antibodies. PLoS pathogens. 2015; 11:e1005110. [PubMed: 26267277]
29. Webb NE, Montefiori DC, Lee B. Dose-response curve slope helps predict therapeutic potency and breadth of HIV broadly neutralizing antibodies. Nature communications. 2015; 6:8443.
30. Walker LM, et al. Broad neutralization coverage of HIV by multiple highly potent antibodies. Nature. 2011 nature10373 [pii].
31. Doria-Rose NA, et al. Developmental pathway for potent V1V2-directed HIV-neutralizing antibodies. Nature. 2014; 509:55–62. DOI: 10.1038/nature13036 [PubMed: 24590074]
32. Mascola JR, Haynes BF. HIV-1 neutralizing antibodies: understanding nature's pathways. Immunological reviews. 2013; 254:225–244. DOI: 10.1111/imr.12075 [PubMed: 23772623]

33. van Esch WJ, et al. Polyreactivity of human IgG Fc-binding phage antibodies constructed from synovial fluid CD38+ B cells of patients with rheumatoid arthritis. Journal of autoimmunity. 2002; 19:241–250. [PubMed: 12473245]
34. Liu M, et al. Polyreactivity and autoreactivity among HIV-1 antibodies. Journal of virology. 2015; 89:784–798. DOI: 10.1128/JVI.02378-14 [PubMed: 25355869]
35. Mian IS, Bradwell AR, Olson AJ. Structure, function and properties of antibody binding sites. Journal of molecular biology. 1991; 217:133–151. [PubMed: 1988675]
36. Sharma SK, et al. Cleavage-independent HIV-1 Env trimers engineered as soluble native spike mimetics for vaccine design. Cell reports. 2015; 11:539–550. DOI: 10.1016/j.celrep.2015.03.047 [PubMed: 25892233]
37. Behrens AJ, et al. Composition and Antigenic Effects of Individual Glycan Sites of a Trimeric HIV-1 Envelope Glycoprotein. Cell reports. 2016; 14:2695–2706. DOI: 10.1016/j.celrep.2016.02.058 [PubMed: 26972002]
38. Wu X, et al. Rational design of envelope identifies broadly neutralizing human monoclonal antibodies to HIV-1. Science. 2010; 329:856–861. [PubMed: 20616233]
39. Scheid JF, et al. Sequence and Structural Convergence of Broad and Potent HIV Antibodies That Mimic CD4 Binding. Science. 2011 science.1207227 [pii].
40. Khayat R, et al. Structural characterization of cleaved, soluble HIV-1 envelope glycoprotein trimers. Journal of virology. 2013; 87:9865–9872. DOI: 10.1128/JVI.01222-13 [PubMed: 23824817]
41. Pritchard LK, et al. Structural Constraints Determine the Glycosylation of HIV-1 Envelope Trimers. Cell reports. 2015; 11:1604–1613. DOI: 10.1016/j.celrep.2015.05.017 [PubMed: 26051934]
42. Sok D, et al. Recombinant HIV envelope trimer selects for quaternary-dependent antibodies targeting the trimer apex. Proc Natl Acad Sci U S A. 2014; 111:17624–17629. 1415789111 [pii]. DOI: 10.1073/pnas.1415789111 [PubMed: 25422458]
43. Garces F, et al. Affinity Maturation of a Potent Family of HIV Antibodies Is Primarily Focused on Accommodating or Avoiding Glycans. Immunity. 2015; 43:1053–1063. DOI: 10.1016/j.immuni.2015.11.007 [PubMed: 26682982]
44. Lee JH, Ozorowski G, Ward AB. Cryo-EM structure of a native, fully glycosylated, cleaved HIV-1 envelope trimer. Science. 2016; 351:1043–1048. DOI: 10.1126/science.aad2450 [PubMed: 26941313]
45. Pettersen EF, et al. UCSF Chimera--a visualization system for exploratory research and analysis. Journal of computational chemistry. 2004; 25:1605–1612. DOI: 10.1002/jcc.20084 [PubMed: 15264254]
46. Van ‘t Wout AB, Schuitemaker H, Kootstra NA. Isolation and propagation of HIV-1 on peripheral blood mononuclear cells. Nat Protoc. 2008; 3:363–370. [PubMed: 18323807]
47. Finzi A, et al. Topological layers in the HIV-1 gp120 inner domain regulate gp41 interaction and CD4-triggered conformational transitions. Molecular cell. 2010; 37:656–667. DOI: 10.1016/j.molcel.2010.02.012 [PubMed: 20227370]
48. Scheres SH. RELION: implementation of a Bayesian approach to cryo-EM structure determination. Journal of structural biology. 2012; 180:519–530. DOI: 10.1016/j.jsb.2012.09.006 [PubMed: 23000701]
49. Scheres SH, Chen S. Prevention of overfitting in cryo-EM structure determination. Nature methods. 2012; 9:853–854. DOI: 10.1038/nmeth.2115 [PubMed: 22842542]
50. Corti D, et al. Analysis of memory B cell responses and isolation of novel monoclonal antibodies with neutralizing breadth from HIV-1-infected individuals. PLoS ONE. 2010; 5:e8805. [PubMed: 20098712]
51. Webb B, Sali A. Comparative Protein Structure Modeling Using MODELLER. Current protocols in bioinformatics/editoral board, Andreas D. Baxevanis … [et al.]. 2014; 47:5 6 1–32. DOI: 10.1002/0471250953.bi0506s47
52. DiMaio F, et al. Atomic-accuracy models from 4.5-A cryo-electron microscopy data with density-guided iterative local refinement. Nature methods. 2015; 12:361–365. DOI: 10.1038/nmeth.3286 [PubMed: 25707030]

53. Chen VB, et al. MolProbity: all-atom structure validation for macromolecular crystallography. Acta crystallographica. Section D, Biological crystallography. 2010; 66:12–21. DOI: 10.1107/S0907444909042073 [PubMed: 20057044]

54. Yasmeen A, et al. Differential binding of neutralizing and non-neutralizing antibodies to native-like soluble HIV-1 Env trimers, uncleaved Env proteins, and monomeric subunits. Retrovirology. 2014; 11:41. [PubMed: 24884783]

55. Yang G, et al. Identification of autoantigens recognized by the 2F5 and 4E10 broadly neutralizing HIV-1 antibodies. The Journal of experimental medicine. 2013; 210:241–256. DOI: 10.1084/jem.20121977 [PubMed: 23359068]

56. Xu Y, et al. Addressing polyspecificity of antibodies selected from an in vitro yeast presentation system: a FACS-based, high-throughput selection and analytical tool. Protein engineering, design & selection : PEDS. 2013; 26:663–670. DOI: 10.1093/protein/gzt047

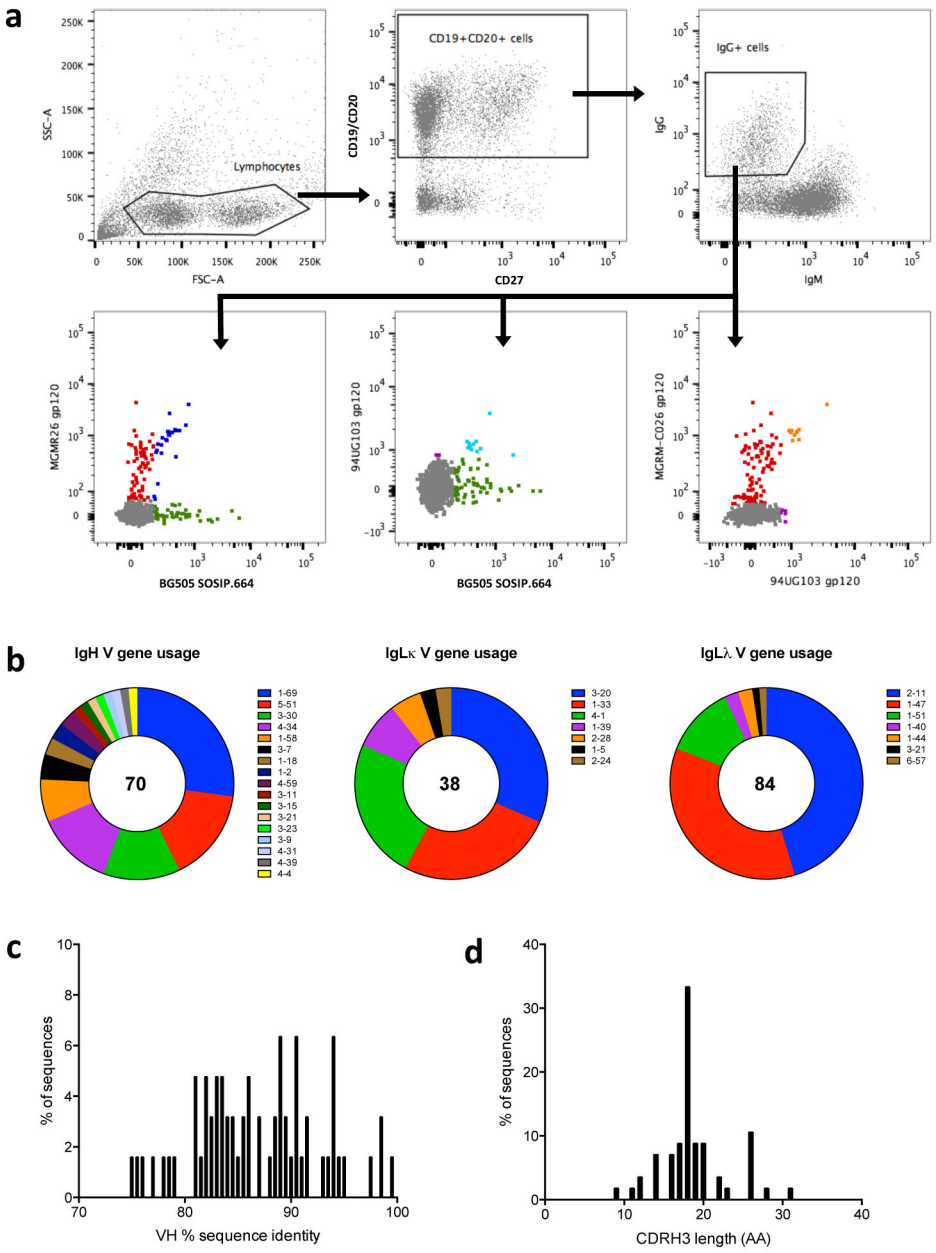

Fig. 1. Isolation and characterization of Env-specific memory B cells from PBMCs of elite neutralizer D12950

(A) PBMCs were gated using the following strategy: negative selection ($CD3^-/CD8^-/CD14^-$), which was followed by positive selection for IgG memory B cells ($CD19^+/CD20^+$) top middle panel ($IgG^+/IgM^-/IgD^-$) top right panel [42]. PBMCs were sorted using BG505 SOSIP.664-AviB trimers (green), 94UG103 gp120-AviB monomers (purple) or MGRM-C026 gp120-AviB monomers (red), double positive for 2 probes (blue, light blue and orange) lower panels. (B) Left panel: In total, 70 heavy-chain sequences were obtained, with a large variation in IgH V gene usage; Middle panel: 38 light-chain kappa sequences; Right panel: 84 light-chain lambda sequences. (C) The heavy-chain sequences are heavily

mutated; most have an average sequence identity frequency of 90% compared to the germline sequence. (D) The CDRH3 length varies, with the average being 18 amino acids.

Clade	n	ACS202	PGV04	PGT121	PGT151	PGT143	VRC026-08
B	10	40%	90%	100%	90%	60%	10%
B (T/F)	9	11%	83%	100%	67%	33%	0%
C	7	86%	50%	83%	67%	50%	83%
C (T/F)	6	50%	50%	33%	33%	33%	50%
BC	6	33%	83%	83%	83%	50%	67%
A	4	25%	100%	50%	75%	25%	50%
CRF02_AG	6	17%	80%	40%	80%	60%	80%
CRF01_AE	9	44%	63%	13%	0%	75%	63%
CRF01_AE (T/F)	4	100%	67%	0%	0%	0%	0%
G, D, CD, AC, ACD	14	43%	69%	54%	69%	38%	54%
Total	**75**	**45%**	**74%**	**56%**	**56%**	**43%**	**46%**

% Neutralization breadth	100%	80%	60%	40%	20%	0%

Clade	n	ACS202	PGV04	PGT121	PGT151	PGT143	VRC026-08
B	10	0.036	0.214	0.031	0.007	0.554	0.940
B (T/F)	9	0.05	0.222	0.026	0.053	0.274	>10
C	7	0.197	0.604	0.153	0.143	0.011	0.004
C (T/F)	6	0.563	0.180	0.033	0.010	0.213	0.025
BC	6	1.708	0.120	0.008	0.004	0.005	0.006
A	4	0.305	0.200	0.027	0.217	0.308	0.065
CRF02_AG	6	0.029	0.421	0.325	0.068	3.340	0.009
CRF01_AE	9	0.306	0.147	2.858	>10	0.054	0.004
CRF01_AE (T/F)	4	0.014	1.245	>10	>10	>10	>10
G, D, CD, AC, ACD	14	0.145	0.040	0.014	0.014	0.032	0.005
Total	**75**	**0.142**	**0.147**	**0.036**	**0.009**	**0.091**	**0.005**

Median IC50 (μg/mL)	0.001	0.010	0.100	1.00	10.0	>10

Fig. 2. Neutralization breadth and potency of bNAb ACS202

Percent neutralization breadth (upper panel) and median IC50 values (based on the viruses that were neutralized; lower panel) obtained when testing ACS202 against a 75-virus panel (Supplementary Table 1). The viruses are grouped by subtype and T/F = transmitted/founder virus and IC50 values and percent neutralization breadth are colored according. bNAbs PGV04, PGT121, PGT151, PGT143 and VRC026-08 serve as comparators for ACS202.

a

	JRCSF mutant	fold reduction ACS202 neutralization	fold reduction PGT121 neutralization	fold reduction PGT151 neutralization
gp120	Q82A	0.5	1.1	ND
	E83A	57	1.0	0.5
	V85A	>61	0.9	ND
	E87A	>61	0.9	10
	T90A*	>61	1.3	56
	N229A	>61	0.8	ND
	N241S*	0.4	1.3	1.1
	N448A*	0.2	0.9	0.7
gp41 FP	A512W	>61	0.8	>240
	V513W	>61	0.6	0.6
	G514W	0.8	0.4	>240
	I515W	15	0.6	0.6
	G516W	>61	0.4	3.7
	A517W	>61	0.7	1.0
	L518W	4.6	0.6	0.7
	F519W	1.2	0.7	1.7
	L520W	>61	0.7	1.4
	G521W	>61	0.8	11
	F522W	5.1	0.7	1.4
	G524W	3.1	1.6	7.4
	A525W	>61	1.1	0.4
gp41 FPPR	S528W	>61	0.5	0.4
	G531W	0.5	0.3	0.4
	A532W	0.6	0.5	1.9
	A533W	35	0.8	>240
	M535W	0.6	0.6	0.3
	T536W	>61	0.7	124
	L537W	53	0.6	>240
	T538W	0.3	0.1	144
	Q540W	2.3	0.8	>240
gp41 HR2	N611A*	0.5	1.6	ND
	N637A*	0.6	0.8	ND

b

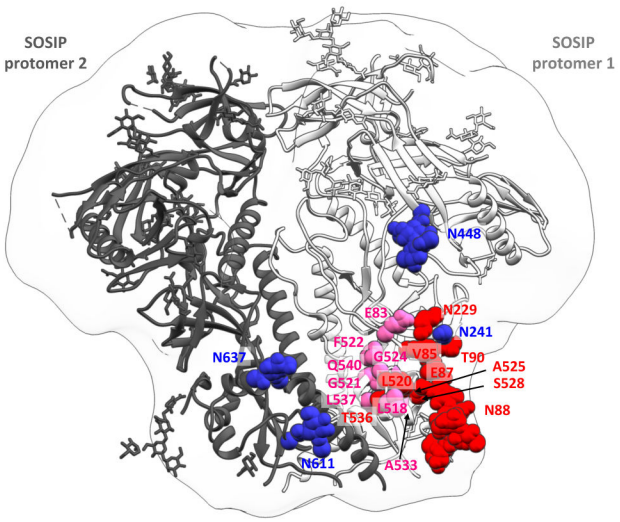

Figure 3. JR-CSF virus mutants affecting ACS202 neutralization

(A) ACS202 neutralization of JR-CSF virus mutants containing the listed single amino-acid substitutions, with those that result in deletion of a glycan site indicated with an *. The values shown are the fold-reduction in neutralization titer for each mutant compared to the wild-type virus (n=3). The color-scheme is based on the intensity of the red shading increasing as the neutralization capacity decreases. The highest ACS202 concentration tested was 10 μg/ml and the IC50 value for ACS202 was 0.083 μg/ml. ND: not determined. FP: fusion peptide. FPPR: fusion peptide proximal region. HR2: Heptad repeat region 2. (B) Mutations that affect the neutralization by ACS202 were modeled onto the crystal structure of BG505 SOSIP.664 trimers in complex with a putative precursor of the PGT121 family (PDB: 5cez). Residue labels denote the corresponding JR-CSF sequence at the modeled BG505 position. Mutations substantially reducing neutralization by ACS202 colored red and pink, while amino acids colored blue had no effect on neutralization when mutated.

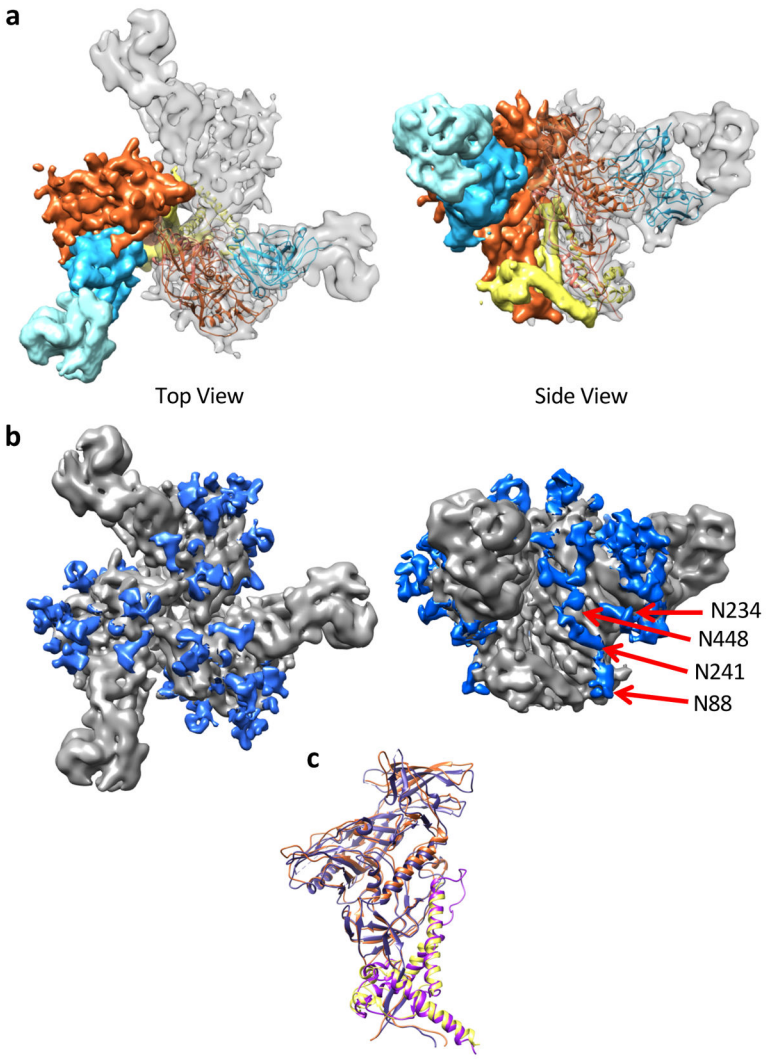

Fig. 4. Cryo-EM structure of AMC011 SOSIP.v4.2 trimers in complex with PGV04 Fab

(A) Top (left) and side (right) views of cryo-EM reconstruction at 6.2 Å resolution. One protomer has been segmented and colored based on domains: gp120 is in orange, gp41 in yellow, variable region of PGV04 Fab in light blue, and the constant region of PGV04 Fab in teal. The adjacent protomer contains a backbone trace of the AMC011 SOSIP.v4.2/PGV04 structure, colored to match the segmented map. (B) Top and side views of the cryo-EM reconstruction with density corresponding to glycans colored in blue with arrows pointing to the N88, N234, N241, and N448 glycans. (C) Superimposition of the AMC011 SOSIP.v4.2 structure (colored as in panel A) with the BG505 SOSIP.664 (PDB: 5CEZ) structure (gp120 dark purple, gp41 light purple). The backbone Cα root mean square deviation (RMSD) between the gp120 domains and the gp41 domains is 1.34 Å and 1.07 Å, respectively.

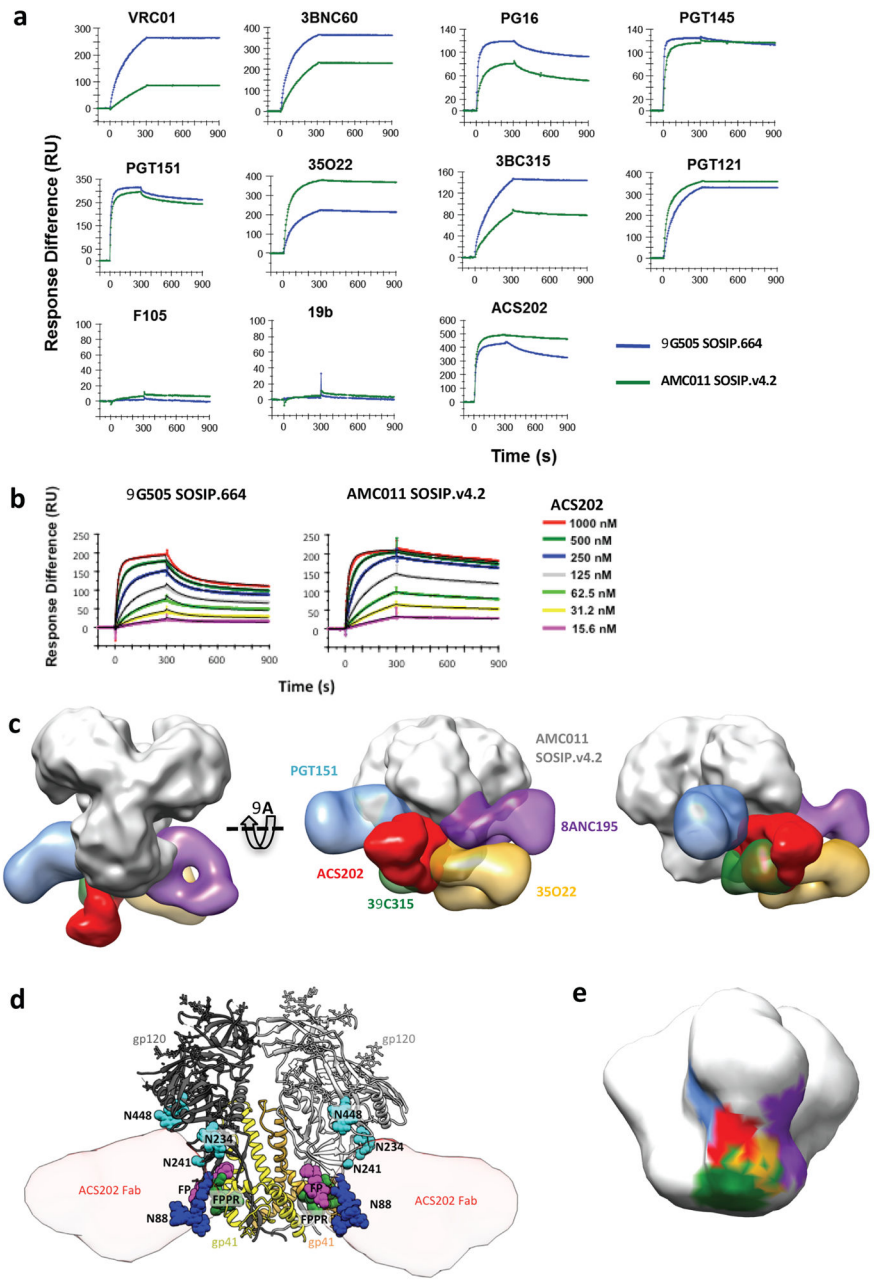

Fig. 5. Antigenicity of AMC011 SOSIP.v4.2 trimers and NS-EM imaging of their complex with ACS202

(A) SPR was used to quantify the binding of the indicated bNAbs and non-NAbs (IgG, each at 500 nM) over a 300 s period to AMC011 SOSIP.v4.2 trimers (green) versus BG505 SOSIP.664 trimers (blue) (data displayed is representative of 2 individual experiments). (B) A dose-range analysis of ACS202-Fab binding to the same trimers (data displayed is representative of 2 individual experiments). (C) Docking of BG505 SOSIP.664 into the EM reconstruction of ACS202 in complex with AMC011 SOSIP.v4.2. Only the EM density for the ACS202 Fab is shown for clarity. The FP and FPPR regions are colored magenta and green, respectively. (E) To estimate the ACS202 epitope footprint, the crystal structure of

anti-RSV antibody AM14 (PDB: 4zyk) was used as the two antibodies have a sequence homology of 80%. (F) 3D model of ACS202 in complex with SOSIP compared to nearby bNAb epitopes. UCSF Chimera [45] was used to dock published EM reconstructions of SOSIP-Fab complexes (PGT151: EMDB-5921; 35O22: EMDB-2672; 8ANC195: EMDB-2625; 3BC315: EMDB-3067) to an EM map constructed using the x-ray coordinates of ligand-free BG505 SOSIP.664 (PDB: 4zmj), low pass filtered to 30 Å. To display the relative docking of Fabs onto the EM reconstruction of AMC011 SOSIP.v4.2 trimers, the "segment map" option was used in UCSF Chimera to isolate the density of the Fab components alone.